Annihilation of edge dislocations in smectic-*A* liquid crystals

M. Ambrožič,[1,2] S. Kralj,[2,3] T. J. Sluckin,[4] S. Žumer,[5,3] and D. Svenšek[5]
[1]*Engineering Ceramics Department, Jožef Stefan Institute, Jamova 39, 1000 Ljubljana, Slovenia*
[2]*Laboratory of Physics of Complex Systems, Faculty of Education, University of Maribor, Koroška 160, 2000 Maribor, Slovenia*
[3]*Condensed Matter Physics Department, Jožef Stefan Institute, Jamova 39, 1000 Ljubljana, Slovenia*
[4]*School of Mathematics, University of Southampton, Southampton SO17 1BJ, United Kingdom*
[5]*Department of Physics, Faculty of Mathematics and Physics, University of Ljubljana, Jadranska 19, 1000 Ljubljana, Slovenia*
(Received 30 October 2003; revised manuscript received 30 July 2004; published 17 November 2004)

This paper presents a theoretical study of the annihilation of edge dislocations in the same smectic plane in a bulk smectic-*A* phase. We use a time-dependent Landau-Ginzburg approach where the smectic ordering is described by the complex order parameter $\psi(\vec{r},t)=\eta e^{i\phi}$. This quantity allows both the degree of layering and the position of the layers to be monitored. We are able to follow both precollision and postcollision regimes, and distinguish different early and late behaviors within these regimes. The early precollision regime is driven by changes in the $\phi(\vec{r})$ configuration. The relative velocity of the defects is approximately inversely proportional to the interdefect separation distance. In the late precollision regime the symmetry changes within the cores of defects also become influential. Following the defect collision, in the early postcollision stage, bulk layer order is approached exponentially in time. At very late times, however, there seems to be a long-time power-law tail in the order parameter fluctuation relaxation.

DOI: 10.1103/PhysRevE.70.051704 PACS number(s): 61.30.Jf, 61.72.Bb

I. INTRODUCTION

At low temperatures, almost all materials exhibit phases with broken symmetries. The low-temperature phase is described by an order parameter which exists on some restricted manifold $\mathcal{D}$. Its local position within $\mathcal{D}$ is then describable in terms of some phase function Φ. The dynamical processes whereby the symmetries are broken are extremely complicated. Almost always the order parameter at one place is different from that at another. The resulting order parameter variation is sometimes relatively strong, but not singular. In this case the order parameter always remains arbitrarily close to $\mathcal{D}$. Defects refer to regions where the phase function $\Phi(\vec{r})$ exhibits singular behavior. They may be points, lines, or surfaces in a bulk system, and it is now known that they may be understood in terms of a topological classification related to the underlying group structure of the order parameter manifold [1,2].

There has long been interest in the physics of defects, long predating the more sophisticated topological studies. Not only do the defects induce long-range forces within a structure, but also the bulk material properties of materials filled with defects can be overwhelmingly dominated by the existence of those defects. For example, it is the presence of dislocations [3] which essentially governs the yield stresses, plastic deformations, and fracture properties in a solid. Likewise, liquid crystal textures [4], which dominate the visual impact of individual liquid crystal phases, are the product of defect structures in the order parameter configurations. The defect structures are thus only a topologically mediated indirect effect of the order parameter manifold itself, but this was nevertheless historically sufficient to identify the nature of the phases [5].

Given their essentially topological basis, it is perhaps not surprising that defect structures exhibit much universality. As a result there are often profound mathematical similarities between apparently completely different physical systems, ranging from condensed matter to cosmological structures [6–8]. These similarities are nevertheless not apparent from a naive nonmathematical point of view.

In this paper we shall be interested in dynamical properties of line defects. This class of defects is represented by disclinations in nematic liquid crystals, in which case they represent singularities in an orientational field, and by dislocations in smectic liquid crystals and solids, which involve singularities in a displacement field. Analogous defect structures are also found in superconductors and superfluids. Our model line defects are edge dislocations in smectic liquid crystals (LCs) [4].

From a practical point of view, the advantage of studying defects in liquid crystals is that the time scale of any motions is many orders of magnitude faster than that in solids. Now interesting effects can be observed on reasonable time scales.

A typical smectic phase consists of a stack of layers, within which there exists liquidlike organization of molecular mass centers [9]. The resulting quasi-two-dimensional system gives rise to logarithmically divergent positional fluctuations with respect to the characteristic sample size. Consequently quasi-long-range positional ordering occurs in finite-sized samples. For all but the mathematical physicist, these systems are one-dimensional solids.

The different smectic phases are classified according to the orientational order within (and between) layers. The simplest phase is the smectic-*A* (Sm*A*) phase. In this, the rodlike molecules tend to be aligned along the layer normal. However, in describing the static and dynamic behavior of edge dislocations in various smectic LC phases the layer ordering plays the dominant role [4,9], while the other degrees of ordering are only of secondary importance. Thus the relatively simple Sm*A* phase, to which we henceforth restrict our

interest, is often sufficient to illuminate the basic mechanisms behind these phenomena.

Edge dislocations in smectics can be induced by a tension that tends to alter the equilibrium layer spacing [10]. These dislocations induce far field stresses and strains, which can be explored using standard liquid crystal elastic theories [9]. But in addition, and of more interest to us here, there is the nature of the dislocation core. In a solid, the dislocation core is best described by the equilibrium positions of the atoms. In a liquid crystal, the density fluctuations underlying the smectic layering undergo a profound rearrangement in this neighborhood, and the relevant structure is represented by an order parameter profile.

There have been a number of attempts to explore defect equilibrium structures in smectics. The crucial input here is the order parameter representing the smectic structure. de Gennes [11] introduced a complex order parameter with a local amplitude and a phase. He drew attention to an analogy between superconducting systems also described by this order parameter. In particular, he pointed out that there might be a smectic analog of the Abrikosov superconducting phase [12], which is defect dominated. Loginov and Terentjev [13] made analytical calculations of the order parameter distribution inside screw and edge dislocations. Analogous calculations have been made by Kralj and Sluckin [14] and by Renn and Lubensky [15], but the details of the structure have not yet been definitively resolved.

Experimental verification is still lacking because of the smallness of the core size. This is typically of the order of a few smectic order parameter correlation lengths. Apart from close to phase transitions this is comparable to a typical molecular size. Edge dislocations can also appear if a change sudden with respect to a relevant smectic ordering relaxation time is imposed on the system. An example is a sudden quench into a smectic phase starting from the isotropic phase.

There have been only a few studies on dynamics of edge dislocations [16–19] in smectics. In these studies the motion of edge dislocations was studied as a function of imposed stress [16–18] and boundary conditions [19]. All these studies employ the classic displacement field description of the smectic ordering, in which order parameter variations are neglected. We shall henceforth refer to this description as the *classical model* [9,20].

This theoretical study concerns the mutual annihilation of edge dislocations lying in the same smectic-*A* phase layer. Now order parameter spatial variations play a necessary role, and so the classic displacement field description is insufficient. Note that in the frame of the classical model the edge dislocations in such a configuration do not interact [21].

We shall describe a system in which two line defects are inserted in the same smectic plane. The layer width far from the defects is equal to the equilibrium one. The equilibrium condition is that the layers attain their natural separations everywhere. Obeying topological requirements this state is obtained via annihilation of dislocations. Our problem is to describe the evolution of the starting system, containing the two dislocations, into the equilibrium system, in which they have disappeared.

The study begins with the order parameter configuration at early times. Here there are two well-defined and well-separated dislocations. At intermediate times, however, the proximity of the dislocations affects the order parameter profiles in each of them. Later still the defects collide and annihilate. However, there is still a ghostlike signature of the previous configuration. Finally all nonequilibrium components of the order parameter decay, leaving a uniform planar smectic bookshelf geometry.

The plan of the paper is the following. In Sec. II we describe our model and the geometry of the problem. In Sec. III, we focus in detail on the annihilation of a pair of edge dislocations. We treat separately the precollision and postcollision regimes. Finally in Sec. IV we summarize our results. Some important details of the study are described in appendixes.

II. MODEL

Our approach is phenomenological, in that we seek equations of motion for the order parameter. Specifically, we shall use the de Gennes complex order parameter to describe the smectic wave. Although this approach has been questioned in recent years [22,23], no superior model exists at the moment. We shall use the Landau–de Gennes free energy [11,13], which we have ourselves used in recent years in a number of studies of inhomogeneous smectic systems [14,24]. In this initial study of smectic defect dynamics we use the most naive time-dependent Ginzburg-Landau approach. This is equivalent to approaches to nematodynamics which ignore backflow. We believe that this will illuminate the most basic features of the problem. In future work we shall return to the problem and attempt to incorporate backflow properly. We now discuss the specific features of the model in more detail.

A. Order parameter

In the Landau–de Gennes approach [11,13] the degree of Sm*A* layer ordering is described by a complex smectic order parameter $\psi=\eta e^{i\phi}$. This quantity corresponds to the first harmonic term in the Fourier expansion in the spatial variation of the molecular mass density ρ. The quantities ψ and ρ are connected through the relation $\rho \approx \rho_0(1+\psi+\psi^*)$, where ρ_0 is the spatially homogeneous density. The modulus η describes the degree of layer ordering, and the phase factor ϕ determines the position of smectic layers. In a homogeneously ordered smectic phase one finds $\phi=\vec{q}_0\cdot\vec{r}$, where the wave vector $\vec{q}_0$ specifies the equilibrium layer spacing $d_0=2\pi/q_0$ and defines the direction of the one-dimensional layering. When this homogeneous smectic is slightly perturbed the phase is commonly expressed with the layer displacement field $u(x,y,z)$ as $\phi(x,y,z)=q_0(z-u(x,y,z))$. The average orientation of molecules within layers is described by the nematic director field $\vec{n}$ pointing along the mean molecular axis. In bulk equilibrium phase the LC molecules point along the layer normal, i.e., $\vec{n}=\vec{q}_0/q_0$.

B. Free energy

The free energy density f of the unconstrained Sm*A* phase contains two terms: f_h and f_e. The first term represents the homogeneous contribution to the free energy density,

whereas the second represents the elastic contribution. The free energy F of the system is obtained by integrating f over the entire volume of the sample:

$$F = \int (f_h + f_e) d^3\vec{r}. \tag{1}$$

For a second order nematic (N) to SmA phase transition the free energy density f_h can be expressed as an expansion in ψ [11]. To lowest relevant order this is

$$f_h = \alpha|\psi|^2 + \frac{\beta}{2}|\psi|^4, \tag{2}$$

where $\alpha = \alpha_0(T - T_{NA})$, α_0, and β are positive material constants, T is the temperature, and T_{NA} the N-SmA phase transition temperature. The minimum of f_h determines the degree of bulk smectic ordering: $\eta_b = \sqrt{\alpha_0(T_{NA} - T)/\beta}$. We neglect coupling between the smectic and nematic order parameters. This can change the order of the smectic-nematic phase transition, but involves physics which is not central to the present purpose.

The elastic contribution of the free energy density f_e describes the elastic response to changes in the smectic ordering. This consists of the nematic ($f_e^{(n)}$) and smectic ($f_e^{(s)}$) components. It is known that the nematic elasticity interacts with the smectic phase to give a second gradient squared term in the displacement in the direction parallel to the smectic layers [13,21]. The resulting long-range strain field is the solution of a quartic equation. However, in order to simplify the problem, in this calculation we shall suppose the director $\vec{n}$ is homogeneously aligned along the direction in which the layers are stacked on average. The result of this assumption is that we can neglect the nematic elastic term $f_e^{(n)}$. Therefore within our approach only the phase factor field ϕ gives rise to the long-range strain field. In Appendix A we show that spatial variations in $\vec{n}$ give rise only to quantitative changes in the behavior of our interest.

The smectic elastic term can be expressed as [9,13,15]

$$f_e^{(s)} = C_\perp |(\vec{n} \times \vec{\nabla})\psi|^2 + C_\parallel |(\vec{n} \cdot \vec{\nabla} - iq_0)\psi|^2. \tag{3}$$

These two terms involve positive elastic constants associated with smectic bend ($C_\perp$) and compressibility ($C_\parallel$). The first term tends to align the smectic layer normal along $\vec{n}$. The smectic compressibility term enforces the layer spacing d_0. Typically the ratio of the compressibility to the bend constant is in the region of 1–10 [9]. In our calculation, for simplicity, we shall take this ratio to be unity and set $C_\perp = C_\parallel \equiv C$. The changes introduced by $C_\perp \neq C_\parallel$ are analyzed in Appendix A.

We now identify the important characteristic lengths that enter our study [9]. These are (a) the smectic layer separation d_0; (b) the separation distance L between defects; and (c) the smectic order parameter correlation lengths $\xi_\parallel = (C_\parallel/2|\alpha|)^{1/2}$ and $\xi_\perp = (C_\perp/2|\alpha|)^{1/2}$.

The quantities $\xi_\parallel$ and $\xi_\perp$ measure the response of the system to locally induced perturbations in the smectic ordering in the directions respectively along the smectic layer ($\xi_\parallel$) and perpendicular to it ($\xi_\perp$). In our calculations, the equality of the elastic coefficients implies that the correlation lengths are also equal, and we set $\xi_\perp = \xi_\parallel \equiv \xi$. Furthermore, so long as order parameter variations can be neglected, as we show in Appendix B, the Euler-Lagrange equation for the variation of the phase factor ϕ alone is scale-free. As a result the variations in ϕ adapt only to the constraints imposed by the geometry of the problem.

C. Dynamics

We adopt the time-dependent Ginzburg-Landau model, in which

$$\gamma \frac{\partial \psi}{\partial t} = -\frac{\delta f}{\delta \psi^*}, \tag{4}$$

where γ represents the effective smectic viscosity constant. The functional derivative with respect to ψ implicitly also includes derivatives with respect to derivatives of ψ. This model has been labeled by Halperin and Hohenberg as model A [25]. Model A usually describes systems in which there is no interaction between order parameter dynamics and classical hydrodynamics. Here it is clear that there are in fact elastic stress tensor terms, and thus strong coupling between hydrodynamics and order parameter relaxation. However, the full inertial dynamical structure has not yet been clarified. Some progress toward this goal has been made by Bruinsma and Safinya [26] and by Brand *et al.* [27]. In the absence of a full and reliable dynamical theory, we restrict the study to order parameter relaxation. We note that in the case of nematic liquid crystals, the effect of ignoring backflow (i.e., hydrodynamic coupling) can in some cases simply change the effective viscosity constant. However in some specific ranges qualitative changes can take place that are not considered in our study [28,29]. An attempt taking into account a flow into the model is demonstrated in Appendix A.

We may remark that this approach is equivalent to making an ansatz for the dissipation function D, and supposing that the free energy gained per unit time is entirely dissipated. Accordingly $-dF/dt = D$, where $D = \int g\, d^3\vec{r}$. The full theory would include inertial effects as well as a more sophisticated formulation of the dissipation function. The simple time-dependent Ginzburg-Landau dissipation function takes the form

$$g = \gamma \left| \frac{\partial \psi}{\partial t} \right|^2, \tag{5}$$

where γ is an effective smectic drag viscosity.

It is now possible to make some initial observations based on dimensional analysis. The characteristic order parameter relaxation time is roughly given by $\tau \sim \gamma/|\alpha|$ and is thus proportional to the square of the smectic order parameter correlation length. By contrast, there is also a time τ_ϕ characterizing distortions in the smectic phase ϕ. This depends on the typical linear size L_d of an imposed distortion. We find that $\tau_\phi \sim \gamma L_d^2/C$, where C stands for an appropriate smectic elastic constant. We develop this argument further in Appendix B.

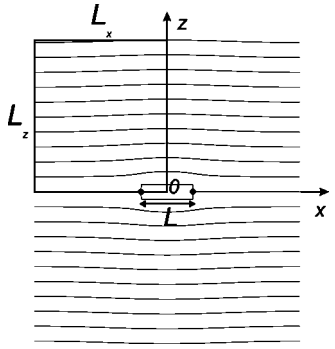

FIG. 1. The geometry of the problem. The edge dislocations are initially separated by a distance L_0. The distances L_x and L_z describe the simulation cell volume. Bold lines indicate the region over which calculations are carried out. Thin lines determine the smectic layers. The two dots mark the centers of defects.

D. Geometry of the problem

The geometry of the problem is depicted in Fig. 1. The smectic layers are stacked along the z axis. The edge dislocations lie along the y direction. The defects are initially separated by a distance L_0, placed symmetrically at $x=\pm L_0/2$ and $z=0$. The presence of the defects gives rise to an elastic displacement field, the value of which is set initially using a mathematical ansatz which we describe in more detail, below. The defects subsequently approach each other along the x axis as shown in the figure. The problem has translational symmetry in the y direction, and we shall suppose that this symmetry is maintained in the solutions. Thus we do not expect spatial variations along the y axis, implying that $\psi(\vec{r})=\psi(x,z)$.

The problem has further reflection symmetry in the $x=0$ and $z=0$ axes. This symmetry permits us to restrict the calculation to a single quadrant, and we choose the quadrant $x<0, z>0$. The region over which calculations are actually carried out is shown in Fig. 1 and is surrounded by bold lines. Only one of the two defects remains in our calculation domain; the behavior of the other can be inferred by reflection symmetry.

We note that the symmetry conditions at the reflection planes $x=0$ and $z=0$ are different. Reflection in the $z=0$ plane leads to the condition $\psi(x,z)=\psi^*(x,-z)$. This is equivalent to the condition $u(x,z)=-u(x,-z)$, where $u(x,z)$ is the displacement of a smectic layer from its equilibrium position. By contrast, reflection in the $x=0$ plane yields the condition $\psi(x,z)=\psi(-x,z)$; this is equivalent to the condition $u(x,z)=u(-x,z)$.

These symmetry relations govern the boundary conditions at the walls of the calculation domain. This domain is cuboid with sides L_x, L_y, L_z. Because of the translational symmetry in the y direction, out of these, only the quantity L_y enters the nondimensionalization.

E. Parametrizations and equations

We use the following nondimensionalizations: (a) The scaled smectic order parameter is $\tilde{\eta}=\eta/\eta_b$; (b) the dimensionless energy is $\tilde{F}=F/F_0$, where $F_0=C\eta_b^2 L_y$; (c) lengths are measured in terms of the smectic order parameter correlation length $\tilde{x}=x/\xi, \tilde{z}=z/\xi, \tilde{L}=L/\xi, \tilde{q}_0=q_0\xi$, etc.; (d) time is measured in units of the smectic order parameter relaxation time $\tilde{t}=t/\tau$.

The scaled order parameter can be expressed as

$$\tilde{\psi}=\tilde{\eta}e^{i\phi}=\tilde{\eta}e^{i[q_0(z-u)]}=\Psi e^{iq_0 z}$$

where far from the defect u represents the conventional layer displacement field. The nonsingular part of the order parameter in the defect region is contained in the exponential $\exp iq_0 z$. All singular contributions giving information about defect structure are contained in $\Psi=\tilde{\eta}\exp[-iq_0 u(x,z)]$. However, in order to circumvent problems with the definition of the phase ϕ where the order parameter is small inside the defect cores, we represent Ψ in terms of its real and imaginary components: $\Psi=\tilde{\eta}e^{-iq_0 u}=A+iB$ [10,24]. In all further calculations we drop all the tildes.

The quantity Ψ is a normalized order parameter which includes the degree of order and departures from perfect smectic order. The free energy can now be rewritten in terms Ψ. The explicit effect of the smectic wave is lost and the theory reduces to the well-known gradient theory with a complex order parameter. The free energy is now

$$f_h=\frac{1}{2}\left(-|\Psi|^2+\frac{1}{2}|\Psi|^4\right), \tag{6}$$

$$f_e=|\nabla\Psi|^2. \tag{7}$$

The time evolution equation (4) can now be written as

$$\frac{\partial\Psi}{\partial t}=2\nabla^2\Psi+\Psi(1-|\Psi|^2). \tag{8}$$

In terms of the parameters $A(x,z,t), B(x,z,t)$, the dynamical Euler-Lagrange equations can be written as

$$\frac{1}{2}\frac{\partial A}{\partial t}=\frac{\partial^2 A}{\partial x^2}+\frac{\partial^2 A}{\partial z^2}+\frac{1}{2}A[1-(A^2+B^2)], \tag{9}$$

$$\frac{1}{2}\frac{\partial B}{\partial t}=\frac{\partial^2 B}{\partial x^2}+\frac{\partial^2 B}{\partial z^2}+\frac{1}{2}B[1-(B^2+A^2)]. \tag{10}$$

F. Boundary and initial conditions

The problem is parabolic in time and ellipsoidal in space. We need to specify initial values $\Psi(x,z,0)$, as well as boundary conditions on the surfaces $z=0, x=0, z=L_z, x=-L_x$. We use the following boundary conditions.

(a) $z=0$. Here the symmetry relation $u(x,z)=-u(x,-z)\Rightarrow u(x,0)=-u(x,0)=0$, i.e.,

$$\frac{\partial A}{\partial z}=0, \quad B=0.$$

(b) $x=0$. Here the symmetry relation is $u(x,z)=u(-x,z)$. Now the condition is that

$$\frac{\partial A}{\partial x}=0, \quad \frac{\partial B}{\partial x}=0.$$

(c) $z=L_z$. There is no symmetry relation, and so we simply suppose that a stable situation has been reached sufficiently far from the defects. This implies that the gradients perpendicular to the wall are zero, or

$$\frac{\partial A}{\partial z}=0, \quad \frac{\partial B}{\partial z}=0.$$

(d) $x=-L_x$. This is analogous to the previous case:

$$\frac{\partial A}{\partial x}=0, \quad \frac{\partial B}{\partial x}=0.$$

We observe, however, that whereas conditions (a) and (b) are set by symmetry, conditions (c) and (d) are set by convenience, and approximate the situation as the distance from the defects approaches infinity. If other plausible conditions are applied on the latter boundaries (e.g., we suppose that they approximate to undisturbed smectic layers) negligible difference in our results is observed.

We use the following initial ansatz for the amplitude and phase of smectic complex order parameter. At the center of the defect we set $\eta=0$. We vary the ordering linearly with the distance from the defect center, reaching the bulk value η_b at the distance equal to the smectic order parameter correlation length. Elsewhere we set $\eta=\eta_b$. For the phase shift we set $\phi=\pi-\varphi$, where $\varphi=\arctan[(z-z_d)/(x-x_d)]$ and the defect is placed at $(x,z)=(x_d,z_d=0)$. This ansatz for the phase shift corresponds to no displacement of layers on the left of the defect and to the half-layer displacement to the right of it. Then the corresponding $A(x,z)$ and $B(x,z)$ profiles are calculated using Eqs. (9) and (10). Quasiequilibrium profiles for relatively large separations L of defects are obtained at a short time relatively to the annihilation time. We also used another initial ansatz for smectic layer displacement [21]. All ansatz profiles have retraced into the same solution after a time period equal to a few correlation times τ.

III. RESULTS

We initially place the edge dislocation at a distance $L=L_0 \gg \xi$ as shown in Fig. 1. The following physical processes then occur.

(i) After a relatively short time, of the order of a few relaxation times, the local core structure reaches the quasiequilibrium order parameter profile.

(ii) From this time on we monitor the annihilation dynamics. In the *precollision regime* well-distinguished defects approach each other to reduce the effective layer curvature of the system. The defects attract because in the absence of the defects the elastic energy is reduced. If the defects approach each other, sufficiently far away, the two defects essentially cancel each other out. If the defects are separated by a distance L, the critical distance over which the defects no longer give rise to a displacement field is of the order of L. The smaller the separation, the smaller the elastic energy.

(iii) The defects then *collide*. In the collision the defects merge and it is no longer possible to distinguish two separate entities.

(iv) In the *postcollision* regime the disturbed structure resulting from the defect collision gradually decays into a bulk, undistorted state.

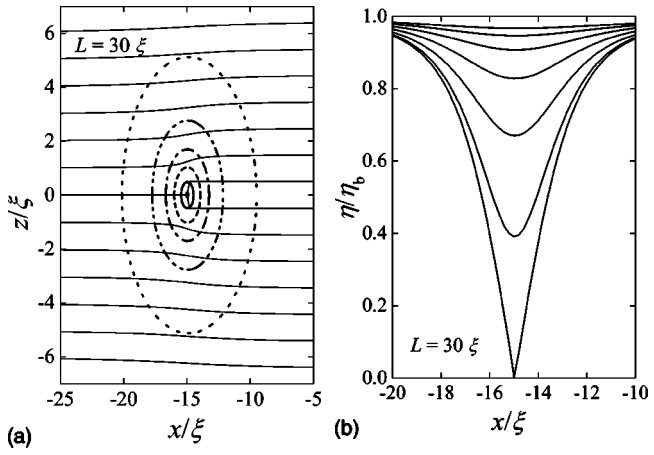

FIG. 2. The order parameter profile of an isolated dislocation located at $z=0$. Left panel: smectic layer profile with contour plot of $\eta(x,z)$ superimposed. Contours correspond to $\eta/\eta_b=0.95$ (dotted line), 0.8 (dash-dot-dotted line), 0.6 (dash-dotted line), 0.4 (short dashed line), 0.2 (solid line), and 0.05 (solid line). Right panel: spatial variation of the order parameter along the x axis at $z=0$, ξ (bottom line), $2\xi,3\xi,4\xi,5\xi,6\xi$ (top line).

We are able further to distinguish in each of the pre- and postcollision regimes two different time regimes, resulting from the different characteristic time scales for η and ϕ. In what follows we analyze in more detail the different stages in the annihilation process.

Some characteristic stages of the annihilation dynamics are shown in Figs. 2 and 3. In the left panel we show the layer profiles with superimposed smectic order parameter contour plots. The contours label the values $\eta/\eta_b=0.95$ (the outermost one), $\eta/\eta_b=0.8$, 0.6, 0.4, 0.2, and $\eta/\eta_b=0.05$ (the innermost one). In the right panel the spatial variation of the order parameter along the x axis is shown at $z=0$ (the bottommost curve), $z=\xi,2\xi,3\xi,4\xi,5\xi$, and $z=6\xi$ (the uppermost curve).

In the *early precollision regime* corresponding roughly to $L>10\xi$, the defects are clearly distinguishable and can be described as linelike objects. On a finer scale, each individual defect exhibits a parasmectic (nearly nematic) region, which extends over a distance of the order of 5ξ. This region defines the defect core. In this regime, the defect cores are not affected by their mutual interaction. A representative order parameter profile of a dislocation is shown in Fig. 2. The spatial profile of η enclosing the melted (nematic) core origin exhibits locally cylindrical symmetry in the (x,z) plane. The cylindrical symmetry is due to the equal elastic constant approximation ($\xi_\perp=\xi_\parallel$). For a real elastic anisotropy, where $\xi_\parallel>\xi_\perp$, the core is extended in the z direction.

With time the defects gradually enter the *late precollision regime*, shown in Figs. 3(a). Now the defect core structure of a defect seems to be influenced by the interaction with its neighbor. The order parameter profiles in the cores gradually lose their cylindrical shape and become extended in the direction joining the defects. The inner contours remain cylindrical, but some outer contours in Figs. 3(a) are now pear

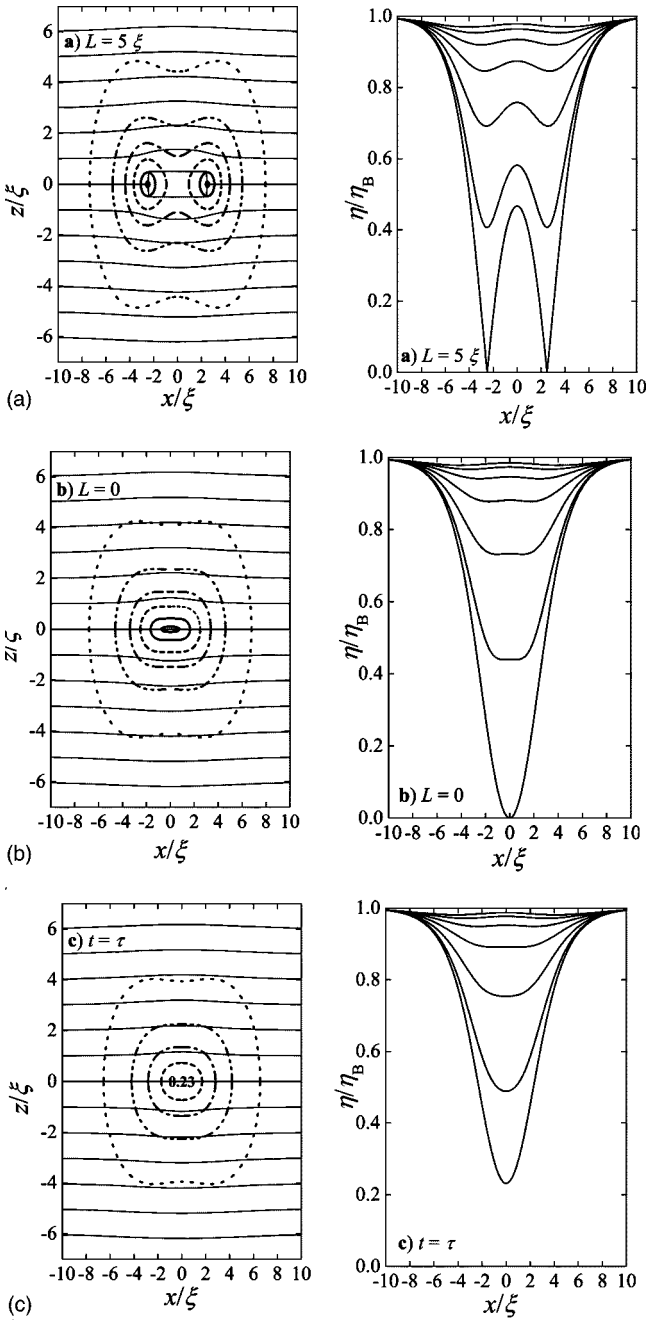

FIG. 3. Order parameter profile at different stages during the annihilation process. Left panel: smectic layer profile with contour plot of $\eta(x,z)$ superimposed. Contours correspond to $\eta/\eta_b = 0.95$, 0.8, 0.6, 0.4, 0.2, 0.05. Right panel: spatial variation of the order parameter along the x axis is shown at $z = 0, \xi, 2\xi, 3\xi, 4\xi, 5\xi, 6\xi$. (a) The late precollision regime, $L = 5\xi$; (b) exactly at the time of collision, $L = 0$; (c) the early postcollision regime, $t = \tau$ and $\eta(0,0)/\eta_b = 0.23$.

shaped, and the very outermost contours even encircle both defects. As the defects further approach, these features become more pronounced, and the departures from a cylindrical shape begin closer and closer to the defect centers, by which we mean the points at which the layering order parameter disappears. Eventually the defect core structures significantly overlap and it is no longer possible to distinguish one from another. Detailed examination of Figs. 3(a) also shows that the time evolution of the outer contours is delayed with respect to those near the defect centers. This is probably the result of a relatively slow layer readjustment which follows from a phase relaxation time-scale $\tau_\phi \sim \gamma L^2/C$. We discuss this point further in Appendix B.

In the *collision*, shown in Figs. 3(b), the melted regions of both defects merge. After this event the "nonsingular" *early postcollision stage* is entered. This stage is characterized by the apparent growth of the order parameter at the collision site on a time scale given by τ. This feature is shown in Figs. 3(c). Gradually the quasiequilibrium order parameter profile is established, adiabatically adjusting to the slower layer displacement dynamics. During this period the degree of layering approaches that expected in an equilibrium smectic phase. Finally, the *late-postcollision stage* is essentially characterized by the layer displacement dynamics, by which the exact thermodynamic equilibrium is asymptotically approached. During this period, the layer displacements disappear.

Next we present a more detailed quantitative picture of the annihilation. In Fig. 4(a) we show the time evolution of the interdefect separation L. The plots for different initial separations L_0 are superimposed. Apart from minor early-time deviations, the curves fall more or less on the same curve. We believe that the initial anomalous $L(t)$ dependence is because the initial ansatz for the defect structure does not correspond to a steady-state solution of Eq. (8), and a short period of relaxation is required. Once the defect core has relaxed, the past history is irrelevant, and subsequent history depends only on present position.

We find that $L(t)$ is rather close to a power-law dependence $L \propto (t_c - t)^\lambda$, where the *collision time* t_c is the time taken until the defects mutually annihilate. The exponent $\lambda \approx 0.5 \pm 0.05$. However, there are small departures from this rule, and the best fitted exponent seems to depend monotonically on the total system size. The value for λ quoted above is an extrapolation to infinite system size. We shall return to the departure from the exact scaling law in the next section.

The initial size-annihilation time dependence law $L(t)$ can be inverted to yield a law for the defect approach velocity $v(L)$. The power law relation $L \propto (t_c - t)^\lambda$ implies an analogous power law relation $v \propto L^{1-1/\lambda}$. Taking the extrapolated $\lambda = 0.5$ suggests the relationship $v \propto L^{-1}$. In Fig. 4(b) we make a log-log plot of the $v(L)$ dependence. One observes a slight change in the behavior when $L(t) \sim \xi$. This is unsurprising, given that structural variations in η near the defects centers become significant.

The asymmetry of the core in this regime is depicted in Fig. 5. One sees that the core size along the z direction remains approximately unaffected and gradually increases in the x direction on approaching t_c. In the mean time the size in the z direction slightly shrinks, revealing the tendency to conserve the amount of the melted region.

An illustrative representation of the characteristic $\eta(t)$ variation is shown in Fig. 6. We plot the time evolution of the order parameter in the middle of the plane through both defects, i.e., $\eta_m = \eta(x = 0, z = 0)$. For $L > 10\xi$ $\eta_m \sim 1$ holds. At later distances (i.e., times) $\eta_m(t)$ monotonically decreases,

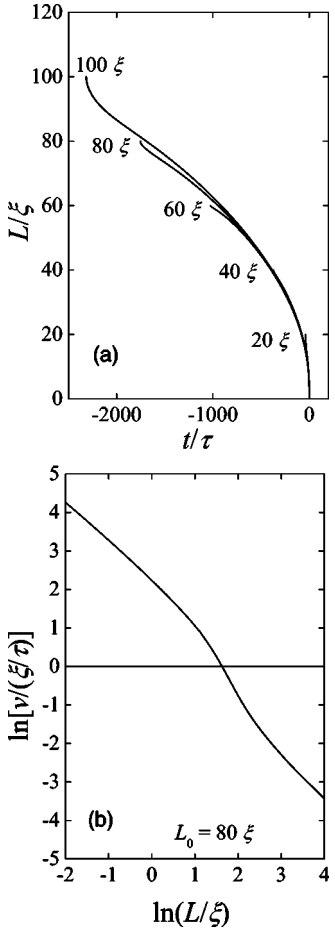

FIG. 4. The dynamics of the precollision regime. (a) The $L(t)$ dependence. Neglecting the initial anomalous dependence we roughly obtain $L \propto \sqrt{(t_c - t)}$. Care should be taken because the observed $L(t)$ dependence on L_0 is due to memory effects. The results are obtained at a temperature where $\xi \sim d_0$. (b) The dependence $v(L)$ on a log-log plot. The law $v \propto 1/L$ would result in a straight line with slope −1.

indicating the merging of the cores of defects. Just before and after the collision the linear dependence $\eta_m \propto |t - t_c|$ is observed. This behavior also emerges from the approximate solution Eq. (11). In it we follow the value of η at the mirror plate at $t < t_c$ and get $\eta_m \propto t_c - t$.

After the collision η_m asymptotically approaches its bulk thermodynamic value η_b. In the late precollision regime the numerical calculations indicate $\eta_b - \eta_m \propto 1/(t - t_c)$. This suggests adiabatic adjusting of η_b to the much slower Φ time evolution.

Note that the edge dislocations in the described geometry do not interact within the classical approach [21]. In our approach the interaction is enabled by the smectic bend elastic term weighted with the elastic constant $C_\perp$ [see Eq. (3)].

IV. DISCUSSION

We first discuss the $L(t) \sim (t_c - t)^{1/2}$ law, which as we have seen above is equivalent to a $v(L) \sim L^{-1}$. We derive a simple ansatz, using Eqs. (9) and (10), which gives insight into the

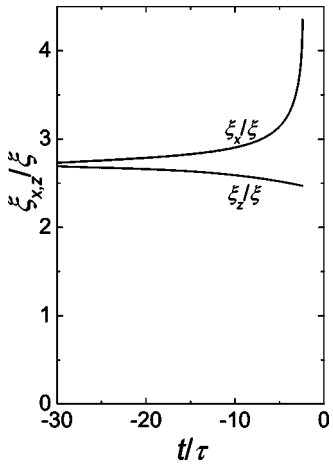

FIG. 5. Precollision regime: the time evolution of the characteristic core size width in the direction along the line connecting the defects and perpendicular to it. The diameters ξ_x and ξ_z, characterizing the core shape, were measured in the x and z directions, respectively, between opposite points at which $\eta = \eta_b/2$.

$L \propto \sqrt{t_c - t}$ dependence. We concentrate on the behavior of $A(x,t)$ at a defect site. Exactly at the defect origin $A = 0$. For $\phi = 0, A = \eta, B = 0$; and $\eta = 0$ at the defect center, but the derivatives of A and B have finite values. Exactly at the defect center, neglecting spatial variations in the z direction (in scaled units), Eq. (9) reduces to $\partial A/\partial t \sim \partial^2 A/\partial x^2$.

A possible solution to this equation is

$$A = c[-(t_c - t) + x^2/2], \tag{11}$$

where c is a constant. The defect position is given by the implicit equation $A(x,t) = 0$. Combining this with Eq. (11) yields

$$x = \sqrt{2(t_c - t)}, \tag{12}$$

which, as shown in Fig. 4(a), describes the whole precollision regime rather well.

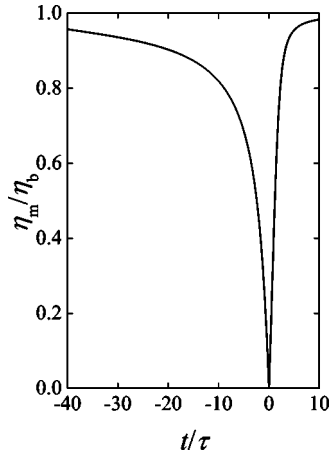

FIG. 6. $\eta(x = 0, z = 0)$ time evolution in the late precollision and postcollision regimes.

It is possible to estimate the experimental time scale corresponding to the cases we have studied. We rewrite Eq. (12) in its dimensional form: $x^2=2(\xi^2/\tau)(t_c-t)\equiv 2D(t_c-t)$, where D plays the role of a diffusion constant. For $D \sim 10^{-12}$ m^2 s^{-1} [18] and ξ of the order of nanometers (which holds true well into the Sm*A* phase), we obtain $\tau \sim 10^{-6}$ s. With this in mind, the longest calculations in Fig. 4(a) extend over a time scale of 10^{-4} s. However, our approach is also applicable close to the *N*-Sm*A* phase transition, where the dynamics is considerably slower. In this regime our calculations may correspond to longer experimentally accessible time scales.

Similar behavior is observed in annihilation of orientational line defects in the nematic and smectic-*C* phases [30–38]. The role of η and ϕ is in this case played by the nematic order parameter and nematic director field, respectively. All these studies, with the exception of Ref. [38], concentrate on the precollision regime. These theoretical, experimental, and simulation studies confirm the basic $L \propto \sqrt{t-t_c}$, i.e., $v \propto 1/L$ behavior. We note that for point defects the balance of forces is different, and in general the $v \sim L^{-1}$ law no longer obtains.

The basic ingredient behind this law has been discussed on numerous occasions [39], and linked to the Peach-Köhler force on dislocations in solids. Let us repeat the argument. The model system is described by the free energy $F=\int K|\nabla\phi|^2 dV$. Here K stands for a representative elastic constant of the LC phase and ϕ is the relevant order parameter field (e.g., the phase factor in a smectic phase or a representative angle of the nematic director field in the nematic phase). The kinetics of the system is governed by the dissipation relaxation law $-dF/dt=D$, where the dissipation function is given by $D=\gamma\int|\partial\phi/\partial t|^2 dV$. The interacting pair of defects are placed along the x axis, separated by a distance L. Then the defect structure survives over a distance of the order of L in all directions, and is quenched on length scales greater than this. Then

$$\frac{\partial\phi}{\partial t}\sim\frac{\partial\phi}{\partial x}v. \tag{13}$$

The dissipation function and the energy function will have the same dependence on separation L, because they are both gradient functions. Let this be $G(L)$. Then

$$G(L)v^2\sim\frac{d}{dt}G(L)\sim\frac{dG}{dL}v, \tag{14}$$

yielding

$$v\sim\frac{d\ln G}{dL} \tag{15}$$

between defects. If $G(L)$ is power law or logarithmic, we obtain $v\sim 1/L$.

Some authors [30–32,34] have derived logarithmic corrections to the basic $v(L)$ law. In general these studies have considered an orientational order parameter, but their considerations probably apply to the present study. Pargellis *et al.* suggested $t_c-t=CL^2[\ln(L/R_c)-0.5]$, which is equivalent to $v(L)\sim(L\ln L)^{-1}$. Here C is a constant and R_c is proportional to the core size of a defect. We do find a better fit to our $L(t)$ results in the early precollision regime with this ansatz, but it requires $R_c \ll \xi$. The significance of this result is unclear.

In a related work [38], some of the present authors have investigated the complete annihilation process of nematic point defects. In this study, using a semimicroscopic lattice-type model and Brownian molecular dynamics, we have found qualitatively similar annihilation (early and late pre- and postcollisional) stages. However, the core structure of nematic point defects in that study was considerably more complex and adopted a ringlike biaxial structure. Other authors [34,36] have also shown that the presence of backflow can significantly change the qualitative picture of final annihilation stages. A particular feature of those studies is the breaking of the mirror symmetry between defects of opposite parity.

Under these circumstances a close analogy between our results and studies of disclination annihilation might well be expected, although naturally some differences would also occur because of the different order parameter symmetries. The index 1/2 nematic disclination and the index 1 *XY* disclination are each minimal from a topological point of view. In the orientational picture the positive and negative index defects are not identical, and thus a breaking of the mirror symmetry in principle is not only possible but expected. However, the mapping of the *XY* model onto a smectic in some sense forces both positive and negative index disclinations to map onto identical dislocations but with opposite Burgers vector, thus restoring the mirror symmetry.

The dynamics of our model is governed by one effective viscosity constant γ introduced by the dissipation term in Eq. (5). This term takes into account only dissipation related to the time changes in the Sm*A* order parameter. It introduces two characteristic time scales τ and τ_ϕ (see Appendix B) that are related to the translational order parameter η and the phase factor ϕ dynamic behavior, respectively. In order to understand microscopic origins of γ we relate the Ginzburg-Landau (GL) model that we use with the classical (CL) model. For the latter model the link with experimental parameters is relatively well established. We originate from Eq. (4), the time-dependent Ginzburg-Landau equation $\gamma\,\partial\psi/\partial t=-\delta f/\delta\psi^*$, describing local changes of the order parameter $\psi=\eta e^{i\phi}$. To take into account flow effects we replace the partial time derivative in Eq. (4) with the material derivative. We get $\gamma\, d\psi/dt=\gamma(\partial\psi/\partial t+\vec{v}\cdot\vec{\nabla}\psi)=-\delta f/\delta\psi^*$, where $\vec{v}$ represents the velocity of the material flow. The CL form of this equation is obtained in the "phase approximation," where spatial variations in η are neglected. We further introduce the displacement field in a "classical way" as $\phi=q_0(z-u)$ and neglect the nonlinear term $\vec{v}\cdot\vec{\nabla}\psi$. The equation $v_z-\partial u/\partial t=-\lambda_p\delta f/\delta u$ follows, which is commonly used to study the dynamics of the displacement field. The quantity $\lambda_p=1/(\gamma q_0^2)$ is known as the permeation constant. The permeation refers to the motion of fluid through the layers. Close to the *N*-Sm*A* phase transition the permeation is particularly easy and $\lambda_p\propto 1/(T_{NA}-T)$. Deep in the Sm*A* phase $\lambda_p \sim d_0^2/\eta_\perp$ holds. Here $\eta_\perp$ describes a fluid viscosity constant along the smectic layer normal. For $T\ll T_{NA}$ the permeation

flow typical length is given by $l_p \sim \sqrt{\eta_v \lambda_p} \sim \sqrt{\eta_v / \eta_\perp} d_0$, where η_v stands for a typical viscous constant. In order to calculate the velocity field [16] the Navier-Stokes equation (in it $\delta f / \delta u$ plays the role of the restoring force) is conventionally used together with the fluid incompressibility condition $\vec{\nabla} \cdot \vec{v} = 0$.

In our approach we neglect the velocity field. If the diffusion within smectic layers, where liquidlike behavior is expected, is an infinitely fast process, only the permeation controls the motion of edge dislocations. But if diffusion cannot relax immediately the vacancies created by permeation the viscosity within smectic layers is also important.

We also believe that the material flow plays a weaker role in the annihilation of smectic edge dislocations in comparison to the annihilation of nematic defects. In the latter case the flow is important and is the main reason behind the asymmetric annihilation process (i.e., the defects with a positive Frank index are faster) of defects. When the nematic defects approach each other, the reorientation of molecules takes place, which is relatively strongly coupled with the fluid flow. In the absence of flow the main source of dissipation is the region surrounding the defects. If the flow is triggered the dissipation is delocalized through the region in which the flow is present. On the contrary the annihilation process of edge dislocations does not require reorientation of LC molecules; therefore the coupling with the flow is weaker. In addition the flow would disrupt smectic layers, which is relatively energetically costly, particularly deep in the Sm*A* phase.

It is possible that our simulation does not appropriately recover events close to the collision of defects, where the relative velocity of defects is very high. The important parameter measuring the credibility of our approach is the so called Deborah number [29] D_e, defined as $D_e = r\tau$. Here r stands for the shear rate and τ is the relevant order parameter relaxation time. If $D_e \ll 1$ then the role of hydrodynamics effects is expected to be negligible. We proceed by estimating the critical velocity v_c for which our calculations are not reliable by requirement $D_e = 1$. We set $r \sim \partial v_x / \partial z$ and τ is the translational order parameter relaxation time. The shear rate is largest close to defects. If we set that the velocity field drops to zero over N_d layers, we get the condition $(v_c / N_d d_0)\tau = 1$. For $\tau \sim 10^{-6}$ s, $d_0 \sim 3$ nm, and $N_d = 3$ we get $v_c \sim 1$ cm/s. This value of velocity is very high. Typically edge dislocations move with the velocity $v < 10^{-2}$ cm/s [18].

Note also that the annihilation is expected to follow a qualitatively different scenario if initially well separated defects (in comparison to ξ) are not in the same plane. Let us assume that they are displaced for a distance Δz and L in the z and x directions, respectively, in the geometry that we use (Fig. 1). In this case the annihilation could be accomplished by a combination of gliding and climbing dynamics. The dislocations are said to *climb* if they move in the smectic plane as opposed to perpendicular to it, representing a *glide*. In a conventional smectic phase a climb of a dislocation is much easier than a glide because a glide necessitates layer breaking. Therefore a relevant characteristic time scale in a layer plane direction and perpendicular to it are expected to be apparently different. The classical theory [4] predicts that the interaction force in the x direction between dislocations can become repulsive for $\Delta_z \neq 0$ for a sufficiently small separation L. Therefore for the case that gliding is apparently less probable than climbing a pair of edge dislocations is expected to get caught in a metastable state at a separation $L = L(\Delta_z)$. The system will then remain in this state until a fluctuation triggers a gliding event, enabling annihilation into the defectless state. In order to simulate this case with our model an anisotropic symmetry allowed dissipation term [see Eq. (5)] including different viscosities in a layer plane and perpendicular to it should be introduced, which is the focus of our future work.

V. CONCLUSION

We have studied the annihilation of edge dislocations in the bulk Sm*A* phase using the phenomenological Landau-Ginzburg approach. We have begun with a pair of facing edge dislocations at a distance $L_0 \gg \xi$. Within the classical approach such dislocations would not interact. In our approach the interaction is enabled by the smectic bend elastic free energy term, weighted by the elastic constant $C_\perp$.

The first stage is an equilibration period taking time ($t \sim 10\tau$), during which the cores relax to an quasiequilibrium profile. We have then followed the dynamics of their mutual annihilation. In the precollision regime the defects were clearly distinguishable. For a large enough initial separation they approached each other in a climbing manner. For sufficiently large initial separation L_0 we find $L \propto (t_c - t)^\lambda$, where $\lambda \sim 0.5$, or equivalently relative velocity $v \propto 1/L$. With decreasing L_0 the effective value of λ seems to decrease monotonically.

We are further able to distinguish between the early and late precollision regimes. In the former regime the defects exhibit nearly symmetric, equilibriumlike core structures. For this case one can treat the defects as linelike objects, which interact via a displacement field that does not affect their internal core structure. In the late precollision regime the cores of defects become modified due to their proximity. When $L < 10\xi$ the cores become extended along the direction of the effective interaction. At the collision time $t = t_c$ the melted centers of both cores merge and defects become indistinguishable. The relaxation after the collision has two qualitatively different stages. In the early postcollision regime the order parameter profile at the collision site exponentially (with characteristic time $\sim 1.5\tau$) approaches the quasiequilibrium $\eta(\vec{r})$ profile, fingerprinting the momentary $\phi(\vec{r})$ pattern. In the late postcollision regime the equilibrium profile is approached as $\eta_b - \eta \propto 1/(t - t_c)$.

Most of our calculations were carried out for the isotropic *XY* limit, where the dynamics of the system is described solely by the complex order parameter ψ. However, we have shown that deviations from this approach in general give rise to relatively small quantitative changes in the behavior of our interest.

ACKNOWLEDGMENTS

This research was supported by an ESF network project COSLAB and Slovenian Office of Science.

APPENDIX A: DEVIATIONS FROM THE ISOTROPIC *XY* BEHAVIOR

In this appendix we estimate how the (i) nematic director field variations, (ii) smectic elastic anisotropy, and (iii) the flow influence the results obtained in the main part of the article.

We first study cases (i) and (ii). We parametrize the director field as $\vec{n}=(\sin\theta,0,\cos\theta)$, where $\theta=\theta(x,z)$. For the sake of simplicity we restrict $\vec{n}$ to vary in the (x,z) plane. In the single Frank nematic elastic constant approximation the nematic elastic free energy contribution is given by $f_e^{(n)}=(K/2)[(\partial\theta/\partial x)^2+(\partial\theta/\partial z)^2]$, where K is the representative Frank nematic elastic constant. The dissipation function of the system [see Eq. (5)] is approximately expressed as $g=\gamma^{(s)}|\partial\psi/\partial t|^2+\gamma^{(n)}(\partial\theta/\partial t)^2$, where $\gamma^{(s)}$ and $\gamma^{(n)}$ approximate the viscosity properties in the smectic and nematic degrees of freedom, respectively. We use the parametrization given in Sec. II E, measure all distances in units of $\xi_\perp$, and we get

$$\frac{1}{2}\frac{\partial A}{\partial t}=c_{xx}\frac{\partial^2 A}{\partial x^2}+c_{zz}\frac{\partial^2 A}{\partial z^2}+\varepsilon c_{xz}\frac{\partial^2 A}{\partial x\,\partial z}+\varepsilon c_x\frac{\partial A}{\partial x}+\varepsilon c_z\frac{\partial A}{\partial z}+c_A, \tag{A1}$$

$$\frac{1}{2}\frac{\partial B}{\partial t}=c_{xx}\frac{\partial^2 B}{\partial x^2}+c_{zz}\frac{\partial^2 B}{\partial z^2}+\varepsilon c_{xz}\frac{\partial^2 B}{\partial x\,\partial z}+\varepsilon c_x\frac{\partial B}{\partial x}+\varepsilon c_z\frac{\partial B}{\partial z}+c_B, \tag{A2}$$

$$\frac{1}{2}\frac{\partial\theta}{\partial t}=\kappa_n\left(\frac{\partial^2\theta}{\partial x^2}+\frac{\partial^2\theta}{\partial z^2}\right)+\frac{c_\theta}{\kappa_\tau}. \tag{A3}$$

Here

$$\varepsilon=\frac{C_\parallel}{C_\perp}-1,\quad \kappa_n=\frac{\gamma^{(s)}K}{\gamma^{(n)}C_\perp\eta_b^2},\quad \kappa_\tau=\frac{\gamma^{(n)}}{\gamma^{(s)}},$$
$$c_{xx}=1+\varepsilon\sin^2\theta,\quad c_{zz}=1+\varepsilon\cos^2\theta,$$

$$c_{xz}=\sin(2\theta),\quad c_x=\frac{\partial\theta}{\partial x}\sin(2\theta)+\frac{\partial\theta}{\partial z}\cos(2\theta),$$
$$c_z=\frac{\partial\theta}{\partial x}\cos(2\theta)-\frac{\partial\theta}{\partial z}\sin(2\theta),$$

$$c_A=q_0B\frac{\partial\theta}{\partial x}[(1+\varepsilon)\cos\theta-\varepsilon\cos(2\theta)]+q_0B\frac{\partial\theta}{\partial z}[-(1+\varepsilon)\times\sin\theta+\varepsilon\sin(2\theta)]+q_0\frac{\partial B}{\partial x}[2(1+\varepsilon)\sin\theta-\varepsilon\sin(2\theta)]+2q_0\frac{\partial B}{\partial z}[(1+\varepsilon)\cos\theta-\varepsilon\cos^2\theta-1]+\frac{1}{2}A[1-(A^2+B^2)]-Aq_0^2[(\varepsilon+1)(1-\cos\theta)^2+\sin^2\theta],$$

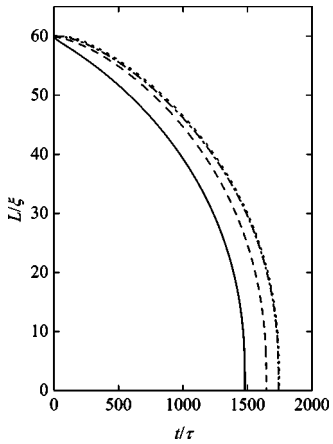

FIG. 7. Influence of elastic anisotropy, nematic distortions, and hydrodynamics on the $L(t)$ dependence. In all cases $L_0=60\xi$. (a) $C_\parallel/C_\perp=1,\kappa_n=\infty$, the solid line; (b) $C_\parallel/C_\perp=5,\kappa_n=\infty$, the dashed line; (c) $C_\parallel/C_\perp=1,\kappa_n=0$, the dotted line; (d) $C_\parallel/C_\perp=1,\kappa_n=\infty$, addition of advection terms, the dash-dotted line. The ratio $a_\parallel/a_\perp=4$, typical for nematogenic molecules, is taken. Note that in cases (c) and (d) the curves nearly overlap.

$$c_B=q_0A\frac{\partial\theta}{\partial x}[-(1+\varepsilon)\cos\theta+\varepsilon\cos(2\theta)]+q_0A\frac{\partial\theta}{\partial z}\times[(1+\varepsilon)\sin\theta-\varepsilon\sin(2\theta)]+q_0\frac{\partial A}{\partial x}[-2(1+\varepsilon)\sin\theta+\varepsilon\sin(2\theta)]+2q_0\frac{\partial A}{\partial z}[-(1+\varepsilon)\cos\theta+\varepsilon\cos^2\theta+1]+\frac{1}{2}B[1-(A^2+B^2)]-Bq_0^2[(\varepsilon+1)(1-\cos\theta)^2+\sin^2\theta],$$

$$c_\theta=\varepsilon c_{\theta1}+(1+\varepsilon)c_{\theta2},$$

$$c_{\theta1}=\left[\left(\frac{\partial A}{\partial z}\right)^2-\left(\frac{\partial A}{\partial x}\right)^2+\left(\frac{\partial B}{\partial z}\right)^2-\left(\frac{\partial B}{\partial x}\right)^2+2q_0\left(A\frac{\partial B}{\partial z}-B\frac{\partial A}{\partial z}\right)+q_0^2(A^2+B^2)\right]\sin(2\theta)+2\left[-\frac{\partial A}{\partial x}\frac{\partial A}{\partial z}-\frac{\partial B}{\partial x}\frac{\partial B}{\partial z}+q_0\left(B\frac{\partial A}{\partial x}-A\frac{\partial B}{\partial x}\right)\right]\cos(2\theta),$$

$$c_{\theta2}=2\left[q_0\left(B\frac{\partial A}{\partial z}-A\frac{\partial B}{\partial z}\right)-q_0^2(A^2+B^2)\right]\sin\theta+2q_0\left(A\frac{\partial B}{\partial x}-B\frac{\partial A}{\partial x}\right)\cos\theta.$$

The dynamics exhibits only relatively small quantitative changes if the nematic distortions or the anisotropy of smectic elastic constants are allowed. This can be inferred from

Fig. 7 where we compare the $L(t)$ dependencies for (a) $C_\parallel/C_\perp=1, \kappa_n=\infty$, (b) $C_\parallel/C_\perp=5, \kappa_n=\infty$, and (c) $C_\parallel/C_\perp=1, \kappa_n=0$. In the limit $\kappa_n=\infty$ the nematic director field is strictly aligned along the z coordinate. For $\kappa_n=0$ the smectic elastic constants dominate the behavior of $\vec{n}$. Therefore $\vec{n}$ is forced to be aligned along the smectic layer normal if $\eta>0$. For conventional LCs one expects $\kappa_n\sim 10$. Note that for $\kappa_n=1$ the characteristic times for the nematic director and smectic phase factor variations are comparable. The case (a) is treated in the main part of the article. Comparison of cases (a) and (c) reveals the magnitude of variations in the $L=L(t)$ dependence if $\vec{n}$ variation is allowed within the model. Note that the time in Fig. 7 is set to zero at the start of the simulation.

Maximal departures of $\vec{n}$ from the z axis take place close to the core of a defect at a distance $z\sim z_d\mp\xi, x=x_d$. The defect is located at $(x,z)=(x_d,z_d)$. Note that exactly at defects the smectic ordering is melted and consequently $\vec{n}$ is there not pushed along the smectic layer normal. In the limit $\kappa_n=0$, where maximal deviations of the director field take place, we get for the maximal tilt angle $\theta_{\max}\sim 30°$. For $\kappa_n=10$ we get $\theta_{\max}\sim 3°$.

We also find that the dynamics in the postcollision regime is negligibly influenced for the described variations.

We have also checked the change of shape of the smectic order parameter contour plots encircling an isolated edge dislocation as the ratio $C_\parallel/C_\perp$ is varied. Circular contours in the case of equal smectic constants are deformed into elliptical ones for $C_\parallel/C_\perp>1$. For $C_\parallel/C_\perp=5$, the ratio between the longest and shortest diameters of the ellipsis roughly equals 2, in line with the scaling prediction $\xi_\parallel/\xi_\perp=\sqrt{C_\parallel/C_\perp}=\sqrt{5}\sim 2.2$.

We next estimate the influence of hydrodynamic flow on $L=L(t)$. For simplicity we set $C_\parallel/C_\perp=1$ and $\vec{n}=(0,0,1)$. The influence of hydrodynamics can be roughly estimated by including advection terms in the dynamical equations for A and B. For this purpose we replace partial time derivatives in dynamical equations with total derivatives. For example in Eq. (8) we introduce the replacement $\partial\psi/\partial t\rightarrow d\psi/dt=\partial\psi/\partial t+(\vec{v}\cdot\vec{\nabla})\psi$, where $\vec{v}$ is the mass flow velocity and $\vec{\nabla}$ stands for the gradient operator.

We consider the case that is schematically shown in Fig. 1, focusing on the defect to the left. The defect is moving to the right, pushing forward the molecules in front of it. These molecules initially constitute the "inserted" layer that gives rise to the pair of defects. In the mean time the molecules from the neighboring layer above (below) the inserted layer move downwards (upwards) to fill the established empty space. Therefore, when a molecule in the inserted layer just in front of the defect moves for a distance $a_\perp$ to the right, the nearby molecules in the surrounding layers move in the vertical direction for a distance $a_\parallel/2$. Here $a_\perp$ and $a_\parallel$ estimate the width and length of a rodlike LC molecule, respectively. If the fluid is incompressible then the velocity field at the defect origin can be approximately expressed as $\vec{v}=v_d(1,0,a_\parallel/2a_\perp)$. Here v_d describes the velocity of the defect. We further assume that the velocity field decays toward zero linearly with the distance $\rho=\sqrt{(x-x_d)^2+(z-z_d)^2}$ from the defect origin. The velocity is set to zero for $\rho\geqslant\xi$. In order to estimate the maximal influence of the advection term we set $(\vec{v}\cdot\vec{\nabla})\psi_i=v_d(1-\rho/\xi)[|d\psi_i/dx|+(a_\parallel/2a_\perp)|d\psi_i/dz|]$ for $\rho<\xi$ and ψ_i stands for either A or B. As shown in Fig. 7 (the dash-dotted line) the influence of the advection term is relatively small.

APPENDIX B: TYPICAL RELAXATION TIMES

We analyze typical relaxation times of a slightly distorted smectic-A phase. We assume that the layers are stacked along the z axis and $\vec{n}=(0,0,1)$. The smectic order parameter is parametrized as $\psi=\eta e^{i\phi}$.

We first consider variations in η and set $\phi=q_0 z$. We expand $\eta=\eta_b+\delta\eta$ about its equilibrium value $\eta_b=\sqrt{-\alpha/\beta}$ up to a quadratic term in $\delta\eta$. With this in mind one gets

$$f\sim f_b(\eta_b)+2|\alpha|\delta\eta^2+C|\nabla\delta\eta|^2, \tag{B1}$$

$$g\sim\gamma\left(\frac{\partial\delta\eta}{\partial t}\right)^2. \tag{B2}$$

The static Euler-Lagrange equation reads $C\nabla^2\delta\eta=2|\alpha|\delta\eta$, defining a typical relaxation distance $\xi=\sqrt{C/2|\alpha|}$.

Neglecting spatial variations the dynamic equation yields $2|\alpha|\delta\eta=-\gamma\partial\delta\eta/\partial t$, defining the relaxation time $\tau=\gamma/2|\alpha|\sim\gamma/|\alpha|$. Note that taking into account spatial derivatives in $\delta\eta$ affects the dynamics only quantitatively. For example, let us take into account in Eq. (B1) spatial variations along the x axis. In typical cases the contribution $C(\partial\delta\eta/\partial x)^2\sim C(\delta\eta/\xi)^2\sim 2|\alpha|\delta\eta^2$ renormalizes the second term in Eq. (B1), leading to $\tau\sim\gamma/4|\alpha|$.

In analyzing the response of the phase factor ϕ we assume a spatially homogeneous profile $\eta(\vec{r})=\eta_b$. Consequently, we get

$$f_e^{(s)}=C\eta^2\left[\left(\frac{\partial\phi}{\partial x}\right)^2+\left(\frac{\partial\phi}{\partial y}\right)^2+\left(\frac{\partial\phi}{\partial z}-q_0\right)^2\right], \tag{B3}$$

$$g=\gamma\eta^2\left(\frac{\partial\phi}{\partial t}\right)^2. \tag{B4}$$

The static Euler-Lagrange equation is now $\nabla^2\phi=0$, which does not introduce any scale into the system. Therefore the variations in ϕ typically adjust to the constraints imposed by boundary conditions.

Let us assume that ϕ evolves over the distance L_d; therefore $f_e^{(s)}\sim C\eta^2(\phi/L_d)^2$. The dynamic equation reads $C\phi/L_d^2=-\gamma\partial\phi/\partial t$, defining the time scale $\tau_\phi\sim\gamma L_d^2/C$.

[1] L. Michel, Rev. Mod. Phys. **52**, 617 (1980).
[2] H.-R. Trebin, Adv. Phys. **31**, 195 (1982).
[3] V. Volterra, Rend. Accad. Naz. Lincei **14**, 351 (1905).
[4] M. Kleman, *Points, Lines and Walls* (Wiley, Chichester, 1983).
[5] G. Friedel, Ann. Phys. (Paris) **18**, 273 (1922).
[6] N. D. Mermin, Rev. Mod. Phys. **51**, 591 (1976).
[7] M. V. Kurik and O. D. Lavrentovich, Usp. Fiz. Nauk **154**, 381 (1988) [Sov. Phys. Usp. **31**, 196 (1988)], and references therein.
[8] http://theory.ic.ac.uk/coslab
[9] P.-G. de Gennes and J. Prost, *The Physics of Liquid Crystals* (Oxford University Press, Oxford, UK, 1993).
[10] M. Slavinec, S. Kralj, S. Žumer, and T. J. Sluckin, Phys. Rev. E **63**, 031705 (2001).
[11] P.-G. de Gennes, Solid State Commun. **10**, 753 (1972).
[12] A. A. Abrikosov, Zh. Eksp. Teor. Fiz. **32**, 1442 (1957) [Sov. Phys. JETP **5**, 1174 (1957)].
[13] E. B. Loginov and E. M. Terentjev, Kristallografiya **30**, 10 (1985) [Sov. Phys. Crystallogr. **30**, 4 (1985)].
[14] S. Kralj and T. J. Sluckin, Phys. Rev. E **50**, 2940 (1994).
[15] S. R. Renn and T. C. Lubensky, Phys. Rev. A **38**, 2132 (1988).
[16] E. Dubois-Violette, E. Guazzelli, and J. Prost, Philos. Mag. A **48**, 727 (1983).
[17] P. Oswald and M. Kleman, J. Phys. (France) Lett. **45**, L319 (1984).
[18] I. Lelidis, M. Kleman, and J. L. Martin, Mol. Cryst. Liq. Cryst. Sci. Technol., Sect. A **330**, 457 (1999).
[19] P. Oswald, P. Pieranski, F. Picano, and R. Holyst, Phys. Rev. Lett. **88**, 015503 (2002), and references therein.
[20] M. Kleman, J. Phys. (Paris) **35**, 595 (1974).
[21] P.-G. de Gennes, C. R. Seances Acad. Sci., Ser. B **275**, 939 (1972).
[22] A. Linhananta and D. E. Sullivan, Phys. Rev. A **44**, 8189 (1991).
[23] M. J. Linehan and G. E. Stedman, J. Phys. A **34**, 6663 (2001).
[24] N. D. Mottram, T. J. Sluckin, S. J. Elston, and M. J. Towler, Phys. Rev. E **62**, 5064 (2000).
[25] P. C. Hohenberg and B. I. Halperin, Rev. Mod. Phys. **49**, 435 (1977).
[26] R. J. Bruinsma and C. R. Safinya, Phys. Rev. A **43**, 5377 (1991).
[27] H. R. Brand, P. K. Mukherjee, and H. Pleiner, Phys. Rev. E **63**, 061708 (2001).
[28] E. I. Kats, V. V. Lebedev, and S. V. Malinin, JETP **95**, 714 (2002), and references therein.
[29] R. F. Bruinsma and C. R. Safinya, Phys. Rev. A **43**, 5377 (1991), and references therein.
[30] H. Pleiner, Phys. Rev. A **37**, 3986 (1988).
[31] A. Pargellis, N. Turok, and B. Yurke, Phys. Rev. Lett. **67**, 1570 (1991).
[32] A. Pargellis, P. Finn, J. W. Goodby, P. Panizza, B. Yurke, and P. E. Cladis, Phys. Rev. A **46**, 7765 (1992).
[33] L. M. Pismen and B. Y. Rubinstein, Phys. Rev. Lett. **69**, 96 (1992).
[34] G. Toth, C. Denniston, and J. M. Yeomans, Phys. Rev. Lett. **88**, 105504 (2002).
[35] A. Bogi, P. M. Lagarde, I. Dozov, and M. Nobili, Phys. Rev. Lett. **89**, 225501 (2002).
[36] D. Svenšek and S. Žumer, Phys. Rev. E **66**, 021712 (2002).
[37] D. Svenšek and S. Žumer, Phys. Rev. Lett. **90**, 155501 (2003).
[38] Z. Bradač, S. Kralj, M. Svetec, and S. Žumer, Phys. Rev. E **67**, 050702(R) (2003).
[39] See, e.g., M. Kleman and O. D. Lavrentovich, *Soft Matter Physics, an Introduction* (Springer, Berlin, 2002), Chaps. 8–10.